Journal of the European Ceramic Society **17** (1997) 1697–1706
© 1997 Elsevier Science Limited
Printed in Great Britain. All rights reserved
PII: S0955-2219(97)00042-3
0955-2219/97/$17.00

Crack Decorating Technique for Fracture-Toughness Measurement in Alumina

Vincenzo M. Sglavo & Paolo Pancheri

Dipartimento di Ingegneria dei Materiali, Università di Trento, Via Mesiano 77, I-38050 Trento, Italy

(Received 27 November 1996; revised version received 10 February 1997; accepted 17 February 1997)

Abstract

A technique for fracture toughness measurement in alumina is presented. Alumina with bimodal grain-size distribution and containing about 10% intergranular glassy phase was used as test material. Controlled defects were introduced by indentation using loads from 1·5 N to 39·2 N. Some specimens were annealed at 1000°C in order to remove the indentation residual stress field. Crack shape and dimension were analyzed by a decorating technique. Red colorant was poured on indented specimens and decorated fracture surfaces were then observed by optical microscopy on later drying. This technique allowed the complete analysis of indentation crack evolution upon bending. Both indented and annealed specimens were considered. Shape-factor evolution during crack growth was investigated and constant fracture toughness values (3–3·5 MPa $\sqrt{m}$*) independent from crack growth and indentation load were calculated.* © *1997 Elsevier Science Limited.*

1 Introduction

Ceramic materials are commonly considered brittle in the sense that stress concentrations generated around defects are not relaxed by plastic flow as well as in ductile materials such as metals and plastics. Therefore, fracture toughness, K_c, represents a critical parameter in the definition of damage resistance and strength of ceramics. From this point of view, the knowledge of K_c becomes important in the comparison among candidate materials for a particular application.

A wide range of methods have been proposed in the past for the determination of fracture toughness. Most of the presented techniques fall into one of the following categories:[1,2]

1. notch methods, in which a saw cut is introduced in the specimen and acts as a sharp crack; chevron notch (CN) and single-edge notch beam (SENB) methods represent two examples;
2. long pre-crack methods, in which a sharp defined crack is generated in the specimen before testing or produced during testing; double cantilever beam (DCB) and double-torsion (DT) methods fall in this category;
3. short pre-crack methods, in which a relatively small crack is introduced before fracture, usually by indentation.

Methods in which the initial defect is introduced by indentation have been extensively studied in the last two decades for several reasons. Rapid test procedures, low cost and ease of testing represent some advantages of the indentation technique. In addition, this technique is a powerful tool for the investigation of fracture process and properties of ceramic materials, starting from flaws similar to natural defects.[2–4] In fact, it is now clear that K_c measurement with such kinds of flaws furnishes results which are usually different from data obtained by tests in which 'long cracks' are used.[3–7]

In most ceramic materials and glasses, Vickers indentation produces four 'radial' cracks which depart from the corner of the indentation site, usually assuming a semi-circular shape around the contact site.[2,8,9] A semi-spherical 'plastic zone' is also formed around the contact site during indentation.[10] The plastic zone is responsible for the presence of a residual stress field which represents the driving force for cracks formation. Apart from radial cracks, 'lateral' cracks develop beneath the plastic zone. These cracks propagate parallel to the surface with a circular front.[2] When an external load is applied to the specimen, for example by bending, radial cracks can lead to sample failure, while lateral cracks, due to their orientation, usually do not participate directly in the fracture process though they can influence radial crack propagation.[11,12]

The stress intensity factor associated with the radial crack system can be expressed as:[2,13–15]

$$K = \chi \frac{P}{c^{1.5}} \quad (1)$$

where P is the indentation load, c the surface crack length and χ a residual stress factor depending on elastic modulus, E, and hardness, H, of the material. The most widely used expression for χ is:[14,16]

$$\chi = \xi \sqrt{\frac{E}{H}} \quad (2)$$

where ξ is a geometrical factor. The coefficient ξ has been evaluated in the past both experimentally and theoretically. Assuming the residual stress field as generated by a 'wedge' between crack faces, Shetty *et al.*[17] calculated a value of 0·014 for ξ. Conversely, Lawn *et al.* proposed a model in which radial crack is subjected to a point force acting on its center and calculated a value equal to 0·023.[16] Experimental determination of ξ has been proposed by Anstis *et al.* who calculated a value of $0{\cdot}016 \pm 0{\cdot}004$.[14]

If an external stress field, σ, is applied to the indented specimen, the stress intensity factor becomes:[2,18,19]

$$K = \chi \frac{P}{c^{1.5}} + \psi \sigma \sqrt{c} \quad (3)$$

where ψ is the shape factor depending on the geometry of the crack and the dimensions of the sample. The shape factor for a semi-circular crack in a semi-infinite solid is equal to 1·29.[9] Nevertheless, due to finite dimensions of the specimens and to crack-shape evolution upon bending, ψ can assume values considerably different.[9,12,20] An important feature is that, when σ increases and the equilibrium condition ($K = K_c$) is reached, the crack undergoes some stable growth before the final failure. In fact, due to the particular form of eqn (3), a crack length interval can be found in which $dK/dc < 0$.[2,18,19] This particular phenomenon has been extensively used to study crack propagation in brittle materials.

Equations (1) and (3) represent fundamental tools for fracture toughness measurement starting from indentation cracks. Fracture toughness can therefore be determined once factors ψ and χ are defined. These parameters are usually considered as constant in conventional indentation fracture mechanics. In addition, indentation cracks are often considered shape-invariant during the propagation process. These requirements are not always fulfilled. Depending on the material and the conditions under which the indentation is performed and stored, crack shape and growth can be complicated by several factors. Environmental effects acting both during and after the indentation process can affect crack shape and residual stress field. Prior to length measurement or bending tests, cracks can grow sub-critically to dimensions sensibly larger than those defined by equilibrium condition [eqn (1)].[9–12,21,22] In addition, the crack shape can change during bending and often flaw size becomes comparable with specimen dimensions. These facts can lead to strong variations in shape factor.

Some procedures have been proposed in recent years in order to quantify the effect of the shape-factor variability and of the residual stress factor in eqn (3). Some authors used Vickers or Knoop indentations to produce surface cracks and residual stress effect was reduced or removed either by annealing or by polishing away the indentation zone.[4,19,23–27] The residual stress factor was, therefore, reduced to zero and the crack geometry for ψ calculation was determined by a decorating technique.[5,28–30] The experimental work required in these procedures is always tedious and quite complicated. In addition, the determination of the exact crack geometry, the interference of lateral cracks and the control of sub-critical growth phenomena represent further difficulties. In other cases, the problem of the determination of ψ and χ was solved by in-situ measurement of crack surface lengths during bending.[3,5] Nevertheless, such procedures required the assumption of some fitting parameters to conduct crack-growth experiments and crack evolution was often referred to the shape of the as-obtained indentation flaw. Moreover, fatigue phenomena which can occur are usually difficult to control.

In this work, precise determination of Vickers indentation crack shape and dimensions is carried out by a decorating technique. This technique is also used to study crack evolution upon bending, thus allowing direct determination of the shape factor as the crack increases. The behaviour of as-obtained and annealed indentation cracks is considered and the effect of the residual stress factor is analyzed. Fracture toughness is then evaluated for different indentation loads.

2 Experimental procedure

Alumina ceramic from a commercial source (ALUBIT 90, Industrie Bitossi, Florence, Italy) was chosen as test material in this work. Alumina is a widely used ceramic material which has been

Table 1. Composition (wt%) of the alumina used in this work

Al_2O_3	SiO_2	CaO	MgO	Na_2O	*Other*
91·7	6·2	0·8	0·5	0·3	0·5

extensively studied in the past. Depending on composition and microstructure, alumina can show specific mechanical properties such as high strength and low flaw tolerance, or relative low strength but decreased dependence of strength on flaw size, due to R-curve behaviour.[27,31–34] The chemical composition of the alumina used in this work is shown in Table 1. Figure 1 shows typical microstructure of this material. Grain-size distribution is bimodal and large elongated grains (up to 20 μm) are immersed in a fine equiaxed grain network (2–5 μm). Sapphire grains are surrounded by an intergranular glassy phase ($\approx$ 10%) which can be removed by treatment in HF water solution.

Test bars (3 mm×4 mm×50 mm) were diamond-machined from plain billets. Edges were chamfered following the prescriptions given in the ASTM norm C 1161–94.[35] The prospective tensile side (4 mm wide) of each specimen was polished with diamond paste to 1 μm finish.

Elastic modulus, E, was measured using a frequency resonance technique.[36] Five different bars were considered and four measurements on each bar were performed. Poisson's ratio equal to 0·23 was assumed in calculations.

Four Vickers indentations (4 mm apart) were introduced using the same load in the central zone of the polished surface of each sample. Maximum contact loads ranging from 15 N to 294 N were used. Impact speed was about 0·5 mm s^{-1}. Indentations were performed in air and maximum load was maintained for 15 s. Specimens were oriented in such a way that the indenter diagonals were parallel to the sample edges.

Indentation site dimensions were measured by an optical microscope and this allowed the determination of Vickers hardness, H. At least five measurements at each indentation load were performed.

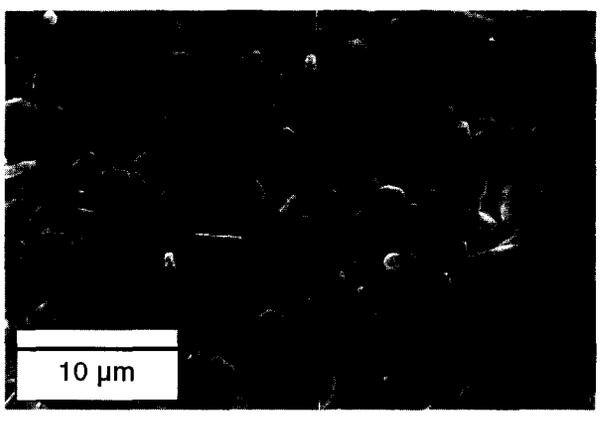

Fig. 1. SEM micrograph showing typical microstructure of the material used in the present work. Intergranular glassy phase was removed by treatment with HF water solution.

Some indented bars were heat-treated at 1000°C for 2 h. Heating and cooling rates lower than 1°C min^{-1} were used. This treatment was performed in order to remove the indentation residual stress field surrounding the indentation flaws. A preliminary study on the stress field around the indentation was performed on the alumina used in this work. An X-ray stress analysis performed by a specifically designed instrument was used for the measurement of residual stresses. These were calculated from the residual strains determined on the basis of (3 1 10) Al_2O_3 peak shift. This analysis showed that heat treatments at temperature in excess of 1000°C are successful for the removal of the residual indentation stress field.[37]

The shape and dimension of the as-obtained indentation cracks were measured using some of the as-indented and annealed specimens. A crack decorating technique was used for this purpose. Some drops of red colorant (CGM, Milan, Italy) diluted with acetone were poured on the indented samples. Red colorant was chosen because this color was seen to make subsequent observation under optical microscope easier. The solution penetrated the surface cracks created during the indenting process. Times around 24 h were shown to be necessary for complete penetration of the red solution into the cracks. The surfaces of the specimens were cleaned and samples were then broken manually using indentation cracks as fracture notches. The red-colored region was observed under an optical microscope equipped with an external white light which was placed beside the specimen. Fracture surfaces were also observed by a scanning electron microscope (SEM).

As-indented and annealed specimens were subjected to four-point bending tests using inner and outer spans of 20 and 40 mm, respectively. Fixtures similar to those described in ASTM C 1161 – 94 norm were used.[35] Care was taken in order to align and center indentations inside the inner span. A cross head speed of 0·2 mm min^{-1} was used. The three indentations on each specimen which did not fail upon bending were used to study stable crack-growth process in as-indented specimens. The same decorating procedure previously described was followed. This analysis was performed also on annealed specimens in order to show any sub-critical or stable growth process.

More detailed information regarding stable crack growth on as-indented specimens was obtained from indented bars subjected to interrupted bending tests. As-indented specimens were loaded using the same four-point bending fixture

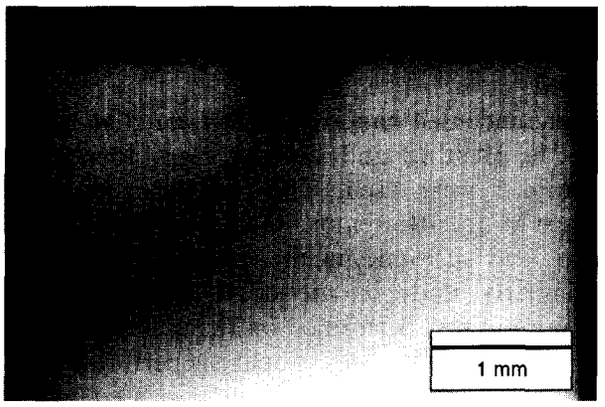

Fig. 2. Optical micrograph of a sub-surface indentation crack obtained with a load of 294 N.

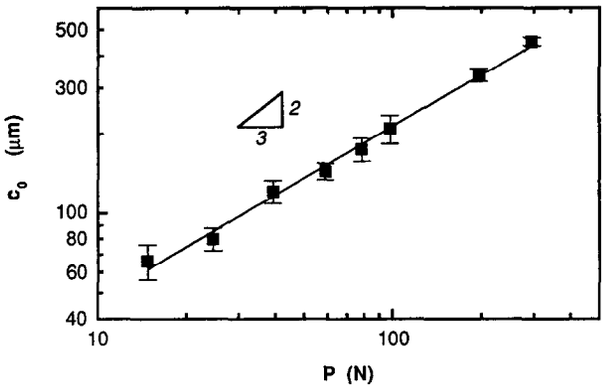

Fig. 4. Surface crack length, c_0 (see Fig. 2), as a function of the indentation load, P. Error bars represent the standard deviation.

previously described to a stress level lower than failure stress and then immediately unloaded. This procedure allowed indentation cracks to undergo some stable growth which was revealed using the same decorating procedure described in the previous sections.

3 Results and discussion

3.1 As-obtained indentation cracks

Elastic modulus, E, and Vickers hardness, H, of the alumina used in this work are equal to 264 ± 4 GPa and $10{\cdot}4 \pm 0{\cdot}6$ GPa, respectively.

The crack decorating technique previously described allowed the measurement of indentation flaw shape and dimension. As-obtained indentation cracks were usually semi-circular or slightly semi-elliptical, the major axis lying on the surface of the specimen. Figure 2 shows an indentation crack obtained with a load of 294 N. A typical semi-circular shape can be observed. Unfortunately, an optical micrograph does not allow one to appreciate in great detail the crack front. Conversely, the crack front is extremely clear when observed directly under a good quality optical microscope where red color makes a bright contrast with the white color of alumina. As-obtained indentation cracks were also analyzed by SEM. In some cases, the crack front appeared well defined due to optimal relative orientation of indentation crack and surrounding fracture surface. Figure 3 shows an SEM micrograph corresponding to a semi-circular indentation crack obtained at 294 N. SEM observations confirmed size measurements performed under optical microscope. Surface crack length, c_0 (see Fig. 2), as a function of the contact load, P, is plotted for as-obtained indentation cracks in Fig. 4. The slope of the fitting curve is equal to 0·65, which is very close to the value 2/3 expected on the basis of conventional indentation fracture mechanics.[2,13,14]

Similar observations were performed on annealed specimens. Indentation cracks subjected to annealing process revealed shape and dimensions similar to as-obtained flaws. Figure 5 shows a typical indentation crack obtained with a load of 294 N and subjected to annealing process. On the basis of the observation of annealed indentation cracks, it can be stated that no crack healing takes place during treatment for 2 h at 1000°C in the alumina used in this work.

Further information regarding processes occurring upon annealing can be obtained if plastic-zone

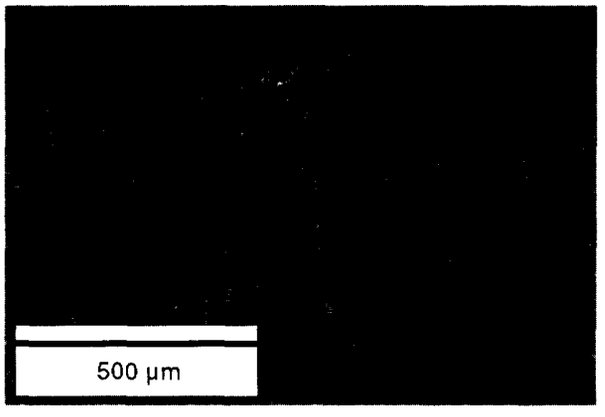

Fig. 3. SEM micrograph showing sub-surface indentation crack obtained with a load of 294 N.

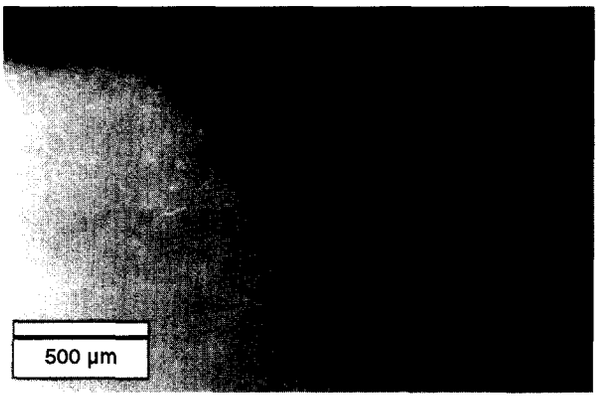

Fig. 5. Optical micrograph of a sub-surface indentation crack obtained with a load of 294 N and subjected to an annealing treatment at 1000°C for 2 h.

evolution is considered. It is a well known fact that in as-indented specimens, the portion of material beneath the contact site is subjected to compressive stresses.[8,15] This zone, depending on the material, is usually characterized by irreversible deformations, such as densification, crushing and compaction or shear faults.[10] Therefore, the sintering and densification process upon heating can be promoted at high temperature. Conversely, zones corresponding to radial crack are subjected to tensile stresses. These oppose the eventual healing process. Decorating technique used for crack-size analysis allows one to point out plastic-zone consistency before and after the annealing treatment. Red colorant poured on as-indented and annealed specimens intensively penetrates the plastic zone (Figs 2 and 5). These micrographs reveal that zones beneath indentations in annealed specimens are strongly colored in the same way as in as-indented samples.

These observations are particularly important to understand failure behavior in annealed specimens when an external stress is applied. Two different models can be proposed to describe fracture behavior of annealed indentation cracks subjected to an external load. To a first approximation, the plastic zone after annealing can be regarded as a semi-circular bridge across the indentation crack which is stretched upon bending. Nevertheless, due to the presence of numerous cracks within the bridge, its strength is limited. In this situation, when an external stress is applied, the bridge is immediately broken and, therefore, the contribution to the overall fracture toughness is low.[2,38] On the other hand, an annealed indentation crack can be approximated to a semi-toroidal crack and the stress-intensity factor upon bending can be evaluated on the basis of the arguments proposed by Moss and Kobayashi.[39] The largest stress intensity always occurs on the inner edge of the crack, i.e. on the border of the former plastic zone. Depending on indentation load, the ratio between inner and outer radius varies from 0·4 to 0·25. If the free surface effects are neglected for simplicity, the ratio between stress intensity factors acting on the inner and outer edge, respectively, varies from $\approx$ 1·4 to $\approx$ 1·2, the larger value corresponding to a higher indentation load. When an increasing external stress is applied, failure initially starts in correspondence with the inner edge and the semi-toroidal crack grows into a semi-circular crack. At this point, stress must be increased further in order to propagate the semi-circular crack and break the specimen. These arguments allow one to consider annealed indentation cracks simply as semi-circular or semi-elliptical upon bending.

3.2 Strength and crack evolution upon bending

Bending strength, σ_f, for as-indented and annealed samples as function of contact load is plotted in Fig. 6. For annealed samples, strength and indentation load are related by P in the relation:

$$\sigma_f P^{1/3} = \frac{K_c^{4/3}}{\psi} \tag{4}$$

Therefore, if K_c and ψ are constant, a linear relation exists between P and σ_f in a logarithmic diagram. The slope of the fitting curve for annealed specimens in Fig. 6 is extremely close to the value of $-0{\cdot}33$ defined in eqn (4). Conversely, for as-indented specimens, the trend of σ_f as a function of P significantly deviates from the slope calculated starting from eqn (3) for ceramic with constant toughness. In this case, if both ψ and χ are constant, at instability, eqn (3) becomes:

$$\sigma_f P^{1/3} = \frac{3}{\psi \chi^{1/3}} \left(\frac{K_c}{4}\right)^{4/3} \tag{5}$$

Therefore, for constant toughness materials, the product $\sigma_f P^{1/3}$ is a constant also for as-indented specimens. Deviation of log σ_f versus log P fitting line to slopes smaller than $-1/3$ is usually taken as evidence of R-curve behavior. Such behaviour has been observed by O'Donnell *et al.* on alumina with bimodal grain-size distribution, similar to the material used in this work.[34] O'Donnell *et al.* demonstrated that the presence of large grains is responsible for the grain bridging mechanism and therefore for R-curve behavior. Deviation from $-1/3$ slope was also observed on coarser grain alumina by several other authors.[27,31,33] At this point, it is important to emphasize that eqn (5) requires that ψ and χ are constant to deduce R-curve behavior. Nevertheless, some recent papers showed that both shape and residual stress factors

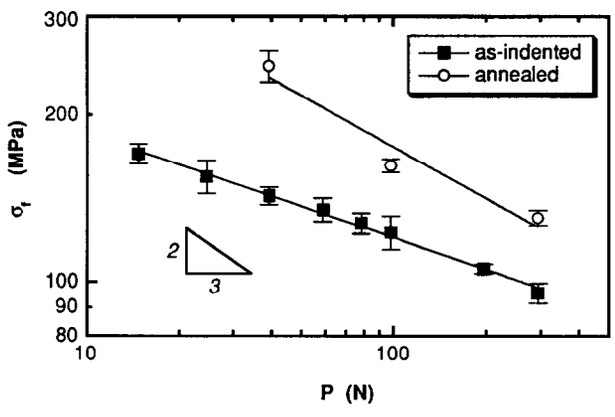

Fig. 6. Bending strength, σ_f, as a function of the contact load, P, for as-indented and annealed specimens. Error bars represent the standard deviation.

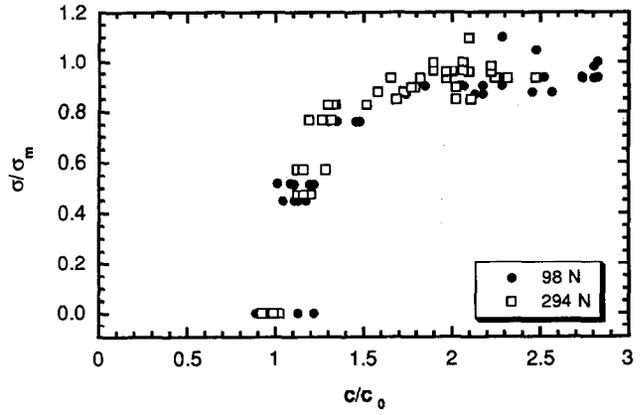

Fig. 7. Normalized plot of the evolution of crack length during stable growth process for indentation cracks obtained at 98 and 294 N.

can vary during indentation crack growth.[9,12,20] Therefore, exact conclusions from Fig. 6 about fracture toughness trend as a function of crack size can be drawn only on the basis of precise determination of ψ and χ as crack growth proceeds.

Crack decorating technique allowed to study the crack-propagation process upon bending. As-obtained cracks were shown to undergo some stable growth before reaching the critical size. When an external stress is applied to an indented specimen, the semi-circular crack grows into a marked semi-elliptical shape, this process becoming more evident for higher indentation loads. Complete evolution of crack size as a function of applied stress is shown in Fig. 7. Crack length at instability is about 2·5 times the initial size, in agreement with indentation fracture mechanics principles.[2,18,19] Figure 8 shows the semi-elliptical shape of a dummy indentation crack produced with a load of 294 N. Crack size at instability as a function of the indentation load is shown in Fig. 9. The depth and the surface length of the crack are indicated with a_m and c_m, respectively. The ellipticity at instability, $e_m = c_m/a_m$ increases for higher indentation loads. These results are consistent with arguments presented by Newman and Raju for

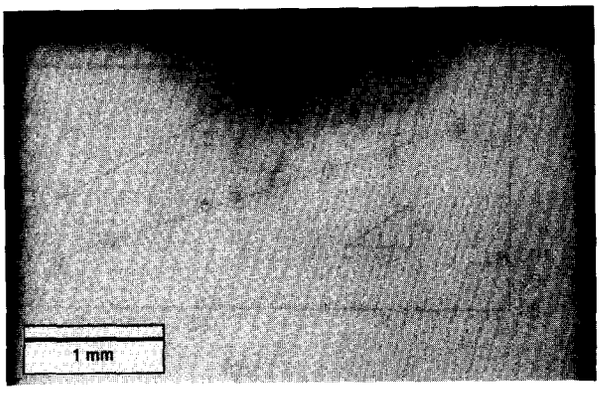

Fig. 8. Optical micrograph showing the sub-surface profile of a dummy indentation crack after stable growth obtained with a load of 294 N.

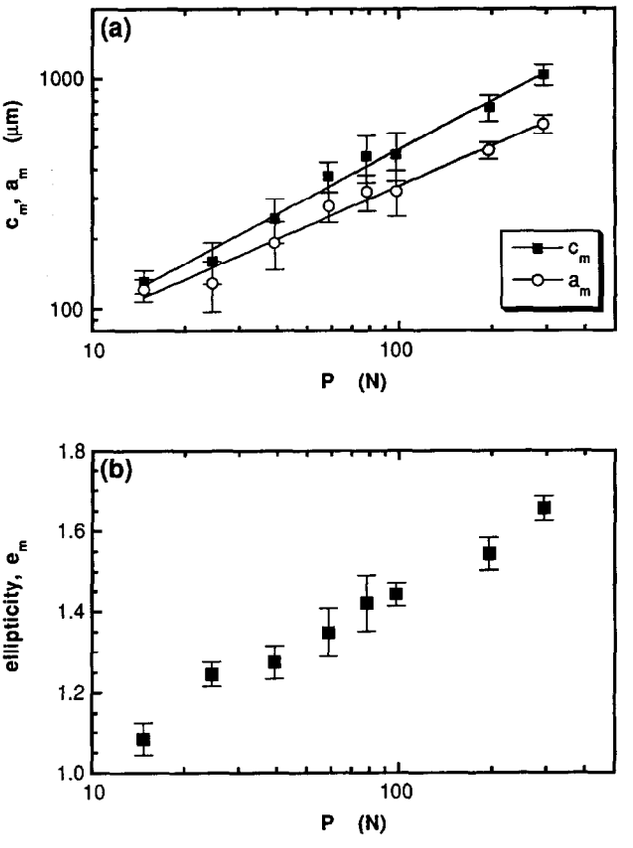

Fig. 9. Crack sizes at instability, a_m and c_m, (a) and ellipticity at instability, e_m, (b) as function of the contact load, P. Error bars represent the standard deviation.

surface cracks in finite plates under bending loads.[40] Stress intensity factor is a variable function on the front of a semi-circular crack in a bar subjected to bending. Stress intensity factor can be expressed as:

$$K = f\sigma\sqrt{c} \tag{6}$$

where σ is the maximum stress acting on the bar, c is half of the surface length and f is a shape factor depending on the dimensions of the crack and the specimen. On the basis of Newman and Raju results,[40] K can be calculated at various locations on the crack front. For semi-circular cracks, K is maximum on the surface and minimum at the maximum depth. If an indentation crack produced with a 15 N load is considered, values of f equal to 1·24 and 1·15, can be calculated for locations on the surface and at maximum depth, respectively. In addition, larger differences can be obtained when bigger cracks are considered. For an indentation crack obtained with $P = 294$ N, f values become 1·18 and 0·96, respectively. Therefore, cracks obtained with larger indentation loads are more prone to evolve into semi-elliptical shapes.

Described evolution for indentation cracks is responsible for shape-factor changes as crack length increases in a stable fashion in as-indented

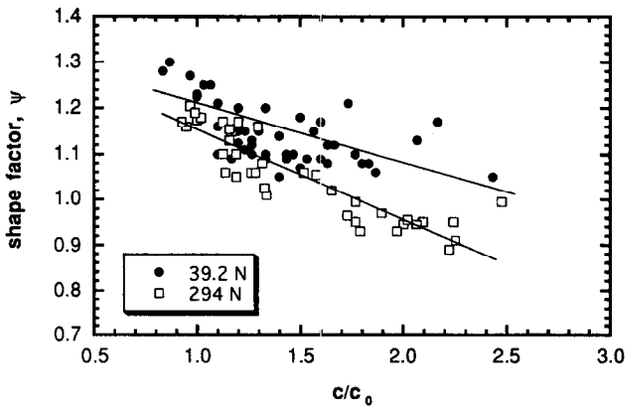

Fig. 10. Shape factor, ψ, evolution during stable growth for indentation crack obtained at 39·2 and 294 N.

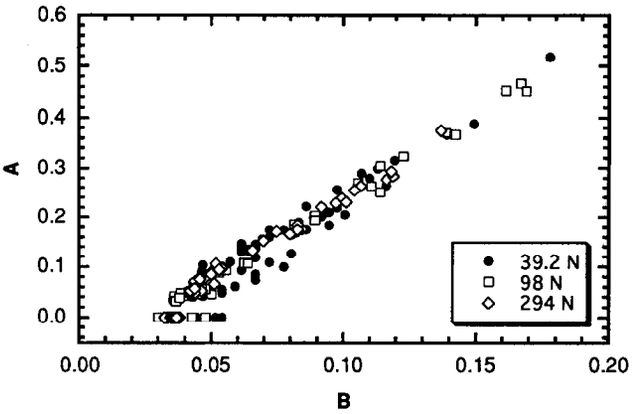

Fig. 11. Plot of $A = \psi\sigma c^2/P$ as a function of $B = c^{1.5}/P$ for three different indentation loads.

specimens. Shape factor was evaluated[40] at each stage of stable growth. Figure 10 shows ψ values as function of surface crack length, c for indentation loads equal to 39·2 and 294 N. Shape factor is a decreasing function of crack size, this trend being more pronounced for higher indentation loads.

Different behaviour was shown by annealed specimens. No evidence of stable growth was observed. In addition, in order to demonstrate that sub-critical growth was not affecting accurate strength measurements, some specimens were subjected to flexure using cross-head speed ranging from 20 μm min^{-1} to 20 mm min^{-1}. Observation of dummy indentations demonstrates that cracks maintain the initial shape up to failure. In addition, strength was always equal to that measured at 0·2 mm min^{-1}. As pointed out previously, there are differences in the shape factor associated with cracks obtained using different indentation loads. Therefore, one would expect that eqn (4) is not fulfilled as P changes. Nevertheless, on the basis of the calculations performed previously, differences between shape factors corresponding to 15 N and 294 N, respectively, are lower than 5% and, indeed, hidden by experimental scatter.

3.3 Fracture-toughness evaluation

Analysis of crack evolution during bending tests can be used for fracture toughness determination. To this purpose, eqn (3) is transformed as:

$$\frac{\psi\sigma c^2}{P} = K_c \frac{c^{1.5}}{P} - \chi \qquad (7)$$

Experimental results from interrupted bending tests, initial and critical crack measurements can be introduced into eqn (7) by the terms $A = \psi\sigma c^2/P$ and $B - c^{1.5}/P$. Once a bending test is interrupted at the applied stress $\sigma(0 \leq \sigma \leq \sigma_f)$, surface length c and depth a are uniquely defined. Using Newman and Raju arguments,[40] shape factor can be calculated. In this way, A and B are determined. Figure 11 shows values of A as a function of B for indentation loads equal to 39·2, 98 and 294 N. A linear trend is evident for all indentation loads. On the basis of eqn (7), experimental data were interpolated by a linear function, thus allowing the determination of fracture toughness and residual stress factor from the slope and the intercept of the interpolating function, respectively. It is important to point out that this procedure is rigorous only if both K_c and χ are independent from crack size. From an analytical point of view, this assumption is reasonable because if K_c was an increasing function of crack length, χ should increase as well in order to maintain the linear trend shown in Fig. 10.

However, no physical reasons can be found to explain an increase of indentation residual stress for larger crack size. Conversely, χ could be a decreasing function of crack length but, in that case, it would be unrealistic to accept K_c as a decreasing function of c. Therefore, both K_c and χ have to be considered as invariant with crack size during stable growth of indentation crack for the material used in this work. This result is particularly important, especially with regard to fracture toughness. The fact that K_c does not increase as the crack propagates means that no toughening effects take place as it will be experimentally demonstrated in detail in the following section. On the other hand, the fact that the residual stress factor remains constant is in agreement with results presented by Sglavo and Green[12] who demonstrated experimentally that χ is invariant during the first stages of indentation crack propagation in soda-lime silicate glass.

Values of K_c and χ obtained from interpolation of data shown in Fig. 10 are reported in Table 2.

Table 2. Fracture toughness, K_c, and residual stress factor, χ, calculated for as-indented specimens

P (N)	K_c (MPa$\sqrt{m}$)	χ
39·2	3·48 ± 0·14	0·12 ± 0·01
98	3·34 ± 0·06	0·10 ± 0·01
294	3·30 ± 0·07	0·09 ± 0·01

Both fracture toughness and residual stress factor are independent from indentation load. Values of χ can be discussed with reference to eqn (2). If the values of elastic modulus and hardness measured for the alumina considered in this work are used, a value of ξ ranging from 0·018 and 0·022 can be calculated. These values are in good agreement with a residual stress factor value experimentally determined by Anstis *et al.*,[14] therefore confirming the independence of χ from indentation load.

Fracture toughness can be evaluated also from annealed specimens. As pointed out previously, in this case, failure occurs in an unstable manner. Therefore, K_c can be calculated by the relation:

$$K_c = \psi \sigma_f \sqrt{c_i} \tag{8}$$

where σ_f is the strength and c_i the crack length. Crack-shape factor was calculated in the usual way[40] and results from bending tests and crack-size measurements were introduced into eqn (8). Fracture toughness equal to $3{\cdot}49 \pm 0{\cdot}22\,\mathrm{MPa}\sqrt{m}$, $3{\cdot}00 \pm 0{\cdot}08\,\mathrm{MPa}\sqrt{m}$ and $3{\cdot}35 \pm 0{\cdot}11\,\mathrm{MPa}\sqrt{m}$ were obtained at indentation loads of 39·2, 98 and 294 N, respectively. These results are almost in agreement with K_c values measured on as-indented specimens.

Fracture-toughness values can be compared to results previously obtained on similar materials and discussed in terms of microstructure. It is important to point out that calculated fracture toughness is independent of crack length. This is in disagreement with results presented by O'Donnel *et al.* for similar glass containing alumina.[34] These authors presented a marked fracture toughness increase as a function of crack size. K_c was shown to change from $2{\cdot}5\,\mathrm{MPa}\sqrt{m}$ at $c = 100\,\mu\mathrm{m}$ to $3{\cdot}5\,\mathrm{MPa}\sqrt{m}$ at $c = 500\,\mu\mathrm{m}$. This R-curve behavior was explained taking into account crack-bridges formation promoted by coarser alumina grains.[34] Observations of interaction between crack front and microstructure in the alumina used in this work allows one to explain the independence of K_c on crack size. Fracture is both intergranular and transgranular, regardless of the size of the grain encountered by the crack front. Despite the presence of large elongated grains, these do not act as bridges for the crack faces. This observation demonstrates the relative high grain boundary fracture toughness which does not allow any grain sliding. The different behavior between the alumina used in this work and that used by O'Donnel *et al.*[34] can be found in the amount and in the composition of the glassy phase. A larger amount of glassy phase and the presence of alkali oxides like Na_2O and MgO can account for a larger strength of the grain boundary glassy phase observed in the alumina used in this work.

At this point, the experimental procedure presented in this work for the determination of K_c can be discussed and compared to similar experimental techniques previously proposed by other authors. Several papers deal with fracture toughness determination from the fracture strength of Vickers indented specimens. In many of these articles, crack shape was assumed as semi-circular and ψ and χ are considered as constant. As already pointed out, these hypotheses sometimes lead to erroneous results. Only in recent years has a tendency to a more accurate evaluation of crack shape been shown. From this point of view, papers by Smith and Scattergood[9] and Steinbrech and co-workers[3,5,29,35] can be considered. These authors presented a similar procedure based on in-situ stable crack-growth technique. Indented specimens were stressed in flexure by a fixture equipped with a microscope which allowed the observation of a stable growth process on the surface. The procedure presented in this work presents some advantages with respect to the method presented by Smith and Scattergood[9] and Steinbrech and co-workers.[3,5,29,35] First of all, the experimental apparatus is particularly simple, consisting only in a bending test device and, separately, in an optical microscope. In this way, crack-size measurement can be performed separately from bending test. An important advantage of this procedure is that measurement of fracture toughness and residual stress factor is possible also at high temperature. A further positive aspect is that sub-critical crack-growth effects can be avoided, due to the possibility of a relative high loading rate upon bending. Therefore, crack growth can be controlled only on the basis of equilibrium condition ($K = K_c$). Finally, the presented procedure allows an exact determination of the indentation crack evolution at each stage of the stable growth process.

4 Conclusions

A simple crack decorating technique for fracture toughness measurement from indented specimens was presented. The procedure was applied to an alumina ceramic. Both as-indented bars and specimens in which indentation residual stress has been removed by annealing were considered. Indented specimens were subjected to bending tests which were interrupted at maximum stress ranging from zero to flexural strength. In this way, a decorating technique allowed one to study the complete evolution of the indentation crack. As-obtained cracks were shown to evolve from a semi-circular shape to a marked semi-elliptical geometry, this phenomenon being more pronounced at higher indentation

loads. Flaws in annealed samples remained semi-circular up to failure. Determination of the crack-shape factor by previous theories allowed the calculation of residual stress factor and fracture toughness. K_c was shown to be invariant with crack length and indentation load, in agreement with observations regarding the interaction of crack front with the microstructure of the material used in this work.

Acknowledgements

The authors thank Professor David J. Green (The Pennsylvania State University) for stimulating discussions. NATO is also acknowledged for partial financial support (CRG 900160).

References

1. Evans, A. G., Fracture mechanics determinations. In *Fracture Mechanics of Ceramics*, Vol. 1, ed. R. C. Bradt, D. P. H. Hasselman and F. F. Lange. Plenum Press, New York and London, 1974, pp. 17–48.
2. Lawn, B. R., *Fracture of Brittle Solids*, 2nd edn. Cambridge University Press, Cambridge, 1993, pp. 35–39.
3. Bleise, D. and Steinbrech, R. W., Flat R-curve from stable propagation of indentation cracks in coarse-grained alumina. *Journal of Am. Ceram. Soc.*, 1994, **77**(2), 315–322.
4. Xu, H. H. K., Ostertag, C. P. and Krause, R. F., Jr, Effect of temperature on toughness curves in alumina. *Journal of Am. Ceram. Soc.*, 1995, **78**(1), 260–262.
5. Steinbrech, R. W. and Schmenkel, O., Crack-resistance curves of surface cracks in alumina. *Journal of Am. Ceram. Soc.*, 1988, **71**(5), C271–273.
6. Lemaitre, P. and Piller, R., Comparison of the fracture toughness of alumina measured by three different methods. *Journal of Mater. Sci. Lett.*, 1988, **7**, 772–774.
7. Murphy, B. R., Predebon, W. W. and Pletka, B. J., The fracture toughness of a high-strength alumina: compact tension versus indentation fracture techniques. *Journal of Mater. Sci. Lett.*, 1994, **13**, 1346–1348.
8. Cook, R. F. and Pharr, G. M., Direct observation and analysis of indentation cracking in glasses and ceramics. *Journal of Am. Ceram. Soc.*, 1990, **73**(4), 787–817.
9. Smith, S. M. and Scattergood, R. O., Crack shape effects for indentation fracture toughness measurements. *Journal of Am. Ceram. Soc.*, 1992, **75**(2), 305–315.
10. Arora, A, Marshall, D. B. and Lawn, B. R., Indentation deformation/fracture of normal and anomalous glasses. *Journal of Non-Cryst. Solids*, 1979, **31**, 415–428.
11. Sglavo, V. M. and Green, D. J., Influence of indentation crack configuration on strength and fatigue behaviour of soda-lime silicate glass. *Acta Metall. Mater.*, 1995, **43**(3), 965–972.
12. Sglavo, V. M. and Green, D. J., The sub-critical indentation fracture process in soda-lime-silica glass. *Eng. Fract. Mech.*, 1996, **55**(1), 35–46.
13. Marshall, D. B. and Lawn, B. R., Residual stress effects in sharp contact cracking. Part 1. Indentation fracture mechanics. *Journal of Mater. Sci.*, 1979, **14**, 2001–2012.
14. Anstis, G. R., Chantikul, P., Lawn, B. R. and Marshall, D. B., A critical evaluation of indentation techniques for measuring fracture toughness. I: direct crack measurements. *Journal of Am. Ceram. Soc.*, 1981, **64**(9), 533–538.
15. Sglavo, V. M. and Green, D. J., Subcritical growth of indentation median cracks in soda-lime-silica glass. *Journal of Am. Ceram. Soc.*, 1995, **78**(3), 650–656.
16. Lawn, B. R., Evans, A. G. and Marshall, D. B., Elastic/plastic indentation damage in ceramics: the median/radial crack system. *Journal of Am. Ceram. Soc.*, 1980, **63**(9–10), 574–581.
17. Shetty, D. K., Rosenfeld, A. R. and Duckworth, W., Analysis of indentation crack as a wedge-loaded half-penny crack. *Journal of Am. Ceram. Soc.*, 1985, **68**(2), C65–67.
18. Marshall, D. B., Lawn, B. R. and Chantikul, P., Residual stress effects in sharp contact cracking. Part 2. Strength degradation. *Journal of Mater. Sci.*, 1979, **14**, 2225–2235.
19. Chantikul, P., Anstis, G. R., Lawn, B. R. and Marshall, D. B., A critical evaluation of indentation techniques for measuring fracture toughness: II: strength method. *Journal of Am. Ceram. Soc.*, 1981, **64**(9), 539–543.
20. Krause, R. F., Jr, Flat and rising R-curves for elliptical surface cracks from indentation and superimposed flexure. *Journal of Am. Ceram. Soc.*, 1994, **77**(1), 172–178.
21. Gupta, P. K. and Jubb, N. J., Post-indentation slow growth of radial cracks in glasses. *Journal of Am. Ceram. Soc.*, 1981, **64**, C112–114.
22. Han, W. T., Hrma, P. and Cooper, A. R., Residual stress decay of indentation cracks. *Phys. Chem. Glasses*, 1989, **30**(1), 30–33.
23. Petrovic, J. J., Jacobson, L. A., Talty, P. K. and Vasudevan, A. K., Controlled surface flaws in hot-pressed Si_3N_4. *Journal of Am. Ceram. Soc.*, 1975, **58**(3–4), 113–116.
24. Quinn, G. D., Kübler, J. J. and Gettings, R. J., *Fracture-Toughness of Advanced Ceramics by the Surface Crack in Flexure (SCF) Method: A VAMAS Round Robin.* VAMAS Technical Working Area 3, Report No. 17, ISSN 1016-2186, 1993.
25. Quinn, G. D., Gettings, R. J. and Kübler, J. J. Fracture-toughness by the surface crack in flexure (SCF) method: Results of the VAMAS round robin. *Ceram. Eng. Sci. Proc.*, 1994, 846–855.
26. Stech, M. and Rödel, J., Method for measuring short-crack R-curves without calibration parameters: case studies on alumina and alumina/aluminum composites. *Journal of Am. Ceram. Soc.*, 1996, **79**(2), 291–297.
27. Braun, L. M., Bennison, S. J. and Lawn, B. R., Objective evaluation of short-crack toughness curves using indentation flaws: case study on alumina-based ceramics. *Journal of Am. Ceram. Soc.*, 1992, **75**(11), 3049–3057.
28. Jones, S. L., Norman, C. J. and Shahani, R., Crack-profile shapes formed under a Vickers indent pyramid. *Journal of Mater. Sci. Lett.*, 1987, **6**, 721–723.
29. Kaliszewski, M. S., Behrens, G., Heuer, A. H., Shaw, M., Marshall, D. B., Dransmann, G. W., Steinbrech, R. W., Pajares, A., Guiberteau, F., Cumbrera, F. L. and Dominguez-Rodriguez, A., Indentation studies on Y_2O_3-stabilized ZrO_2. I; Development of indentation-induced cracks, *J. Am. Ceram. Soc.*, 1994, **77**(4), 1185–1193.
30. Dransmann, G. W., Steinbrech, R. W., Pajares, A., Guiberteau, F., Dominguez-Rodriguez, A. and Heuer, A. H., Indentation studies on Y_2O_3-stabilized ZrO_2. II; Toughness determination from stable growth of indentation-induced cracks. *Journal of Am. Ceram. Soc.*, 1994, **77**(5), 1194–1201.
31. Chantikul, P., Bennison, S. J. and Lawn, B. R., Role of grain size in the strength and R-curve properties of alumina. *Journal of Am. Ceram. Soc.*, 1990, **73**(8), 2419–2427.
32. Cook, R. F., Liniger, E. G., Steimbrech, R. W. and Deuerler, F., Sigmoidal indentation-strength characteristics of polycristalline alumina. *Journal of Am. Ceram. Soc.*, 1994, **77**(2), 303–314.
33. Kovar, D. and Readey, M. J., Role of grain size in strength variability of alumina. *Journal of Am. Ceram. Soc.*, 1994, **77**(7), 1928–1938.
34. O'Donnel, H. L., Readey, M. J. and Kovar, D., Effect of glass additions of the indentation-strength behavior of alumina. *Journal of Am. Ceram. Soc.*, 1995, **78**(4), 849–856.

35. ASTM norm C1161-94, Standard test method for flexural strength of advanced ceramics at ambient temperature. In *Annual Book of ASTM Standards*, Vol. 15.01, American Society for Testing and Materials, Philadelphia, PA, pp. 309–315.
36. ASTM norm C1198-91, Standard test method for dynamic Young's modulus, shear modulus and Poisson's ratio for advanced ceramics by sonic resonances. In *Annual Book of ASTM Standards*, Vol. 15.01, American Society for Testing and Materials, Philadelphia, PA, pp. 332–338.
37. Scardi, P., Leoni, M. and Sglavo, V. M., unpublished results.
38. Becher, P. F., Microstructural design of toughened ceramics. *Journal of Am. Ceram. Soc.*, 1991, **74**(2), 255–269.
39. Moss, L. W. and Kobayashi, A. S., Approximate analysis of axisymmetric problems in fracture mechanics with application to a flat toroidal crack. *Int. Journal of Fracture Mech.*, 1971, **7**(1), 89–99.
40. Newman, J. C. and Raju, I. S., An empirical stress intensity factor equation for the equation for the surface crack. *Engng Fracture Mech.*, 1981, **15**, 185–192.